Article

Current Biology

Contribution of non-sensory neurons in visual cortical areas to visually guided decisions in the rat

Graphical abstract

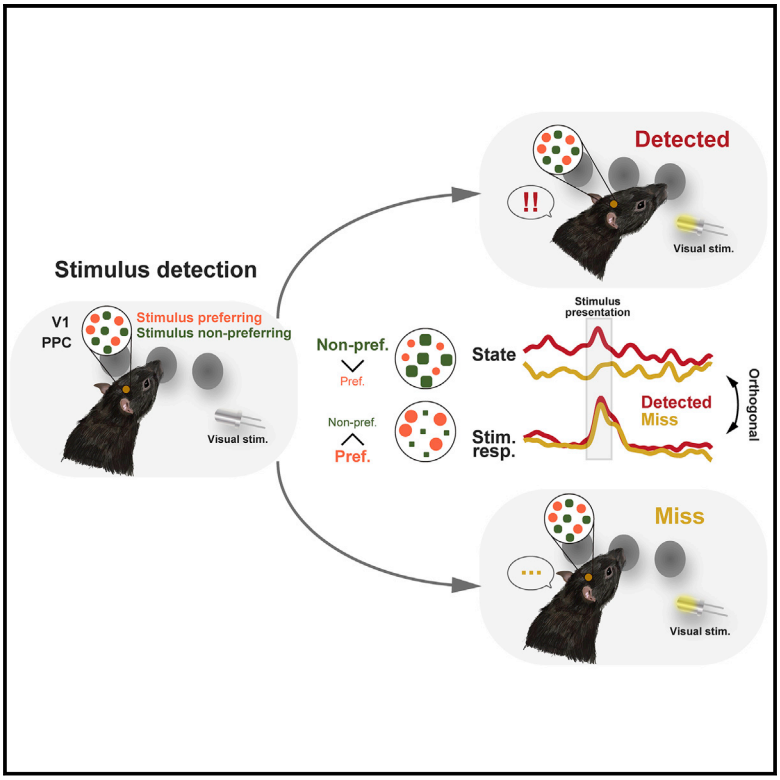

Highlights

- Rats often fail to respond to visual stimuli despite the presence of V1 responses
- State fluctuation, but not visual response, correlates with visual detection
- Stimulus non-preferring neurons in V1 and PPC contribute to state fluctuation
- Stimulus timing relative to state fluctuations in V1 correlates with decision bias

Authors

Yuma Osako, Tomoya Ohnuki, Yuta Tanisumi, Kazuki Shiotani, Hiroyuki Manabe, Yoshio Sakurai, Junya Hirokawa

Correspondence

dddb1003@mail4.doshisha.ac.jp, yyosako@gmail.com (Y.O.), jhirokaw@mail.doshisha.ac.jp (J.H.)

In brief

The trial-by-trial variability in visual detection performance can be attributed to the neural state fluctuations in visual cortical areas. Osako et al. show that stimulus timing relative to the state of the non-sensory neurons in the visual cortical areas segregates visual detection performance via the population-level mechanism.

Osako et al., 2021, Current Biology *31*, 1–13
June 21, 2021
https://doi.org/10.1016/j.cub.2021.03.099

CellPress

Current Biology

CellPress
OPEN ACCESS

Article

Contribution of non-sensory neurons in visual cortical areas to visually guided decisions in the rat

Yuma Osako,[1,3,*] Tomoya Ohnuki,[1] Yuta Tanisumi,[1] Kazuki Shiotani,[1,2] Hiroyuki Manabe,[1] Yoshio Sakurai,[1] and Junya Hirokawa[1,3,*]

[1]Laboratory of Neural Information, Graduate School of Brain Science, Doshisha University, 1-3 Tatara Miyakodani, Kyotanabe, Kyoto 610-0394, Japan

[2]College of Life Sciences, Ritsumeikan University, 1-1-1 Noji-higashi, Kusatsu Shiga 525-8577, Japan

[3]Lead contact

*Correspondence: dddb1003@mail4.doshisha.ac.jp or yyosako@gmail.com (Y.O.), jhirokaw@mail.doshisha.ac.jp (J.H.)

https://doi.org/10.1016/j.cub.2021.03.099

SUMMARY

It is widely assumed that trial-by-trial variability in visual detection performance is explained by the fidelity of visual responses in visual cortical areas influenced by fluctuations of internal states, such as vigilance and behavioral history. However, it is not clear which neuronal ensembles represent such different internal states. Here, we utilized a visual detection task, which distinguishes internal states in response to identical stimuli, while recording neurons simultaneously from the primary visual cortex (V1) and the posterior parietal cortex (PPC). We found that rats sometimes withheld their responses to visual stimuli despite the robust presence of visual responses in V1. Our unsupervised analysis revealed distinct population dynamics segregating hit responses from misses, orthogonally embedded to visual response dynamics in both V1 and PPC. Heterogeneous non-sensory neurons in V1 and PPC significantly contributed to population-level encoding accompanied with the modulation of noise correlation only in V1. These results highlight the non-trivial contributions of non-sensory neurons in V1 and PPC for population-level computations that reflect the animals' internal states to drive behavioral responses to visual stimuli.

INTRODUCTION

Identical sensory stimuli sometimes evoke different perceptual and behavioral responses. For instance, in a sensory detection task, human or animal subjects are instructed or well trained to reliably report the presence or absence of sensory stimuli to obtain rewards. When the sensory stimulus is near the threshold to prompt a decision, subjects' responses vary across trials despite their best efforts to get the reward. Interestingly, even if they report absence of stimuli, it is sometimes possible for them to correctly guess above chance level if they are forced to answer.[1–4] Revealing the neuronal mechanisms underlying such trial-by-trial variability of perceptual responses is crucial to understand how the brain exploits sensory information for optimal decision making.

Trial-by-trial variance of responses to identical stimuli is believed to reflect noise in the conversion of sensory information into motor outputs.[5] It has been demonstrated that the variability of the firing rates of sensory neurons is responsible for the variable response to different choices.[6,7] However, accumulating evidence suggests that perceptual decisions are also significantly affected by latent subjective states reflecting task engagement.[8] For instance, behavioral response variability is correlated with mind wandering in humans[9] and fluctuations of physiological and behavioral states in animals.[10–13] These subjective state drifts could be partially attributed to cortical activity fluctuation.[13–15] The synchronization and desynchronization of many neurons in particular areas of the cortex could affect the efficiency of population coding.[16,17] Accordingly, shared response variability in pairs of sensory neurons (i.e., noise correlation), modulated by attention, arousal, and reward expectation, can affect efficient coding of stimulus features and sensory processing, resulting in behavioral variability in a sensory detection task. Moreover, task engagement is known to be modulated by the trial-by-trial experience of decision making and varying outcomes,[18–24] in turn regulated by distinct neuron populations in association areas.[25–27] Furthermore, some studies have suggested that neurons that do not explicitly respond to a stimulus contribute to texture discrimination in the somatosensory cortex,[28] working memory coding in the prefrontal cortex,[29] stimulus/choice coding in the auditory cortex,[30] and category representation in the prefrontal cortex.[30] These studies highlight the potential contribution of non-sensory neurons to modulating sensory processing. However, how non-sensory neurons coordinate with sensory neurons to optimize sensory decisions is yet unknown.

Numerous studies have revealed that neuronal activity in the primary visual cortex (V1) and posterior parietal cortex (PPC) plays a crucial role in visual detection.[31,32] Patients with V1 lesions reported subjective blindness,[33,34] and direct optogenetic inhibition of rodent V1 impaired visual detection behavior.[35] On the other hand, the PPC is known to play essential roles in

Please cite this article in press as: Osako et al., Contribution of non-sensory neurons in visual cortical areas to visually guided decisions in the rat, Current Biology (2021), https://doi.org/10.1016/j.cub.2021.03.099

selective attention and reward-history bias[27,36] and regulates the response properties of V1 neurons.[37–39] Recent imaging studies have examined visual perceptual behavior during a go or no-go detection task and found that task requirements[40] heavily modulate visual responses in the PPC and that heterogeneous recruitment of V1 neurons plays an important role in visual detection.[40,41] Together, these studies support the notion that the V1 and PPC create distinct cortical states at the population level that integrate task-relevant external signals[42] with internal states for subjective detection performance.

Although neuronal imaging studies addressed population coding of sensory processing across different cortical areas, the go or no-go task paradigm, often used in experiments with head-fixed animals, is susceptible to subjective biases: go trials may contain false alarms and no-go trials may contain misses[43] due to fluctuating internal states, as described above. To further classify such internal states during visual detection, we previously developed a spatial-visual cue detection task for free-moving rats.[1] The task combines a two-alternative spatial choice with a third option for no stimulus, which allowed us to isolate the hit trials less contaminated with false alarms. Furthermore, we utilize a shutter for the central port that enables us to force rats to make spatial choices, even when they initially chose the central port. It separates the miss responses into two distinct categories: "missed responses with the capability to choose the correct side when forced (Miss+)" and "missed responses without the capability to choose the correct side when forced (Miss−)." This allows us to uniquely interrogate how visual information in the visual cortex fails to drive correct choice behaviors by comparing "self-driven correct choice" and Miss+ conditions. By taking advantage of these relatively homogeneous trials with different behavioral responses to identical stimuli, we aimed to reveal the neural mechanisms underlying variable visual detection performance due to subjective biases. We recorded neuronal activity simultaneously from V1 and PPC to test how sensory and non-sensory neurons (hereafter defined as "stimulus non-preferring neurons") in these cortical areas differently contribute to the population-level computation for visually guided decisions.

RESULTS

Rats performed visual detection task based on their internal threshold

We trained seven rats to perform a spatial visual-cue detection task (Figures 1A–1C), which is essentially a three-alternative choice design that encourages animals to report the presence or absence of peripheral visual stimuli as described in our previous study.[1] Briefly, the rats initiated a trial by poking their nose at the central port. They were rewarded by choosing outer ports (left or right) when a visual stimulus was presented or by keeping the nose in the central port when no peripheral stimulus was presented. In half of the trials, the central port was closed 0.5 s after stimulus presentation to force animals to choose one of the outer ports.

To confirm whether rats had a steady choice criterion, we alternated probe sessions with graded stimulus strength (session A) and neuronal recording sessions with a constant near-threshold stimulus strength (session B). In session A, consistent with our previous study,[1] the peripheral choice accuracy in forced-choice (FC) trials decreased from approximately 80% to 65% as visual contrast decreased (Figures 1D, orange, and S1A), and the accuracy was maintained at >90% regardless of visual contrast in the three-choice (3C) trials (Figures 1D, blue, and S1A). Note that trials where rats chose to stay in the central port were excluded from calculating spatial choice accuracy in 3C trials. Rats missed the visual stimuli more often (from 50% to 70%) as visual contrast decreased (Figures 1E, S1B, and S1E). They also showed >90% correct rejection performance when the visual stimulus was omitted in 3C trials (Figures 1F, S1C, and S1E). These results confirmed that rats have a generalized strategy to choose the outer ports in response to peripheral stimuli only when their choice criterion is met. In addition, rats showed correct choices above the chance level when the shutter forced them to select one of the outer ports after first choosing to stay in the central port (Figures 1G, gray, and S1D). Thus, the rats received visual information but did not always maximally exploit it. We labeled trials with different choice types as hit correct (Hit+), hit incorrect (Hit−), miss correct (Miss+), and miss incorrect (Miss−) according to choice performance (Figures 1A and 1B).

To determine what drove the rat's choice, we applied a generalized linear model (GLM) analysis to the behavioral data. We used multiple variables, such as current stimulus, previous reward positions, and previous failure (unrewarded), as independent variables and predicted spatial choice direction and go or no-go responses to left and right stimuli (Figures 1H and S1F, respectively). We compared regression coefficients and uniquely explained variance by the variable (STAR Methods). Note that individual delta-R^2 does not add to the total R^2 because some of the variance can be explained by multiple factors. In the Hit trials, the majority of the spatial choice variance (67%) was accounted by the stimulus direction alone with minimal contributions (2%) from previous reward positions (Figure 1H). In contrast, although the total explained variance was much lower (~30%) in the Miss trials, previous reward positions had a stronger effect on spatial choice (6%; Figure 1H). We also confirmed mild contributions (about 10%) of previous reward positions in go or no-go decisions (Figure S1F). Together, spatial choices in the hit trials were predominantly driven by visual information with little influence of previous reward positions, although spatial choices in the miss trials were partially influenced by the incongruent previous reward positions to the stimuli.

Stimulus-preferring neurons in V1 and PPC were activated regardless of choice types

We recorded neurons simultaneously from the right V1 (N_{V1} = 515 neurons) and right PPC (N_{PPC} = 436 neurons) using chronic tetrode implants during task performance (Figure S3E). To investigate how visual neuronal responses contribute to behavioral responses, we first identified stimulus-preferring neurons using time-locked kernel regression analysis with multiple task predictors, such as contra- and ipsi-lateral stimuli, motor preparation, and choice-preparation kernels (Figures 2A and S3A–S3C; STAR Methods). Approximately 30%–40% of the neurons were defined as selective to visual stimulus in V1 (40%; N = 203) and PPC (27%; N = 116; Figures 2B–2D and S3C). Based on the results, we classified the neurons as

Please cite this article in press as: Osako et al., Contribution of non-sensory neurons in visual cortical areas to visually guided decisions in the rat, Current Biology (2021), https://doi.org/10.1016/j.cub.2021.03.099

CellPress
OPEN ACCESS

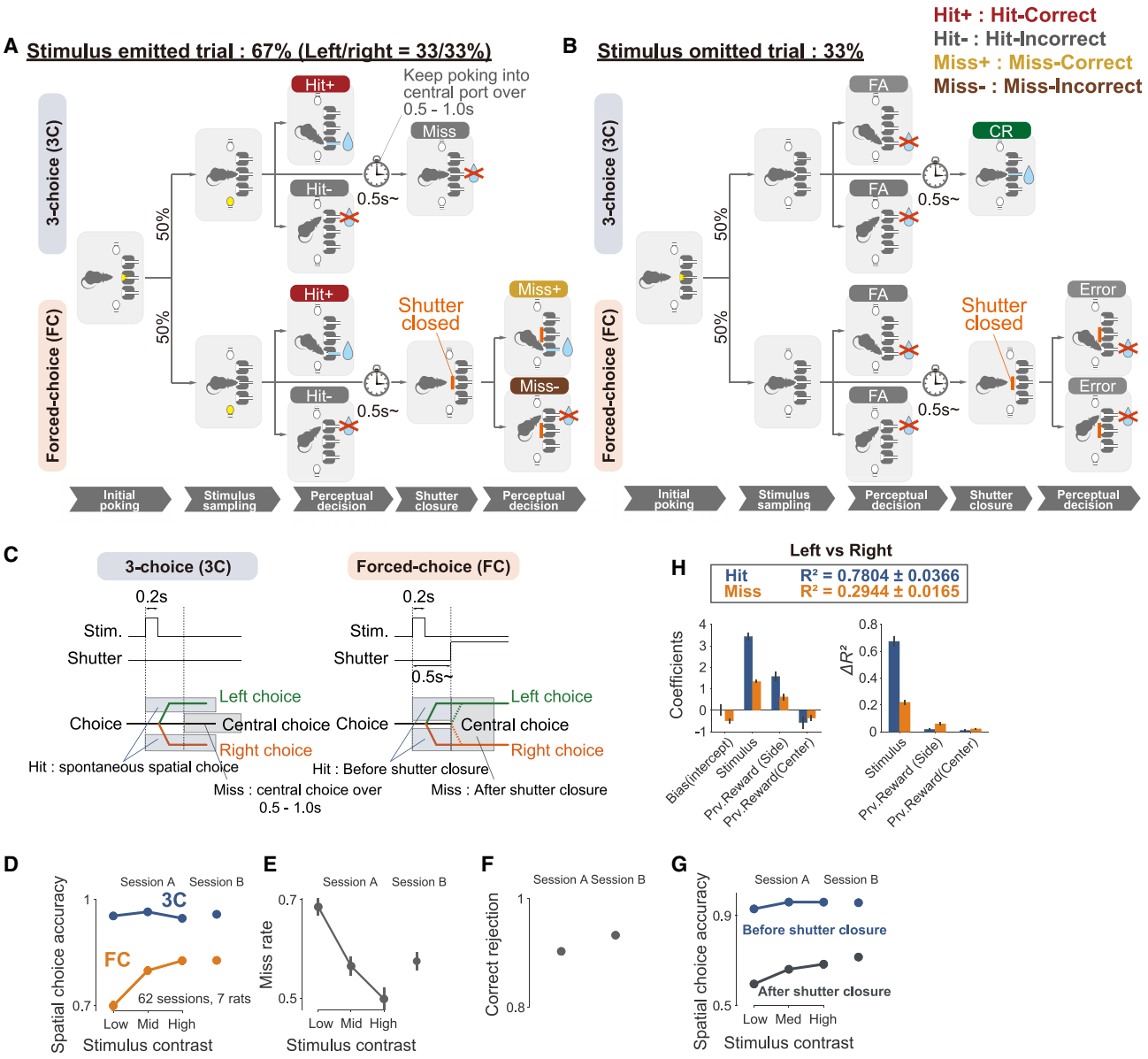

Figure 1. Spatial visual-cue detection task

(A and B) Schematics of the behavioral paradigm. Rats initiated a trial by nose poking into the central port and waited for 0.2–0.6 s to receive a peripheral stimulus. Rats were rewarded by poking into the corresponding port when the peripheral stimulus was presented (A) or into the central port when the stimulus was not presented (B).

(C) Task timeline. Rats were free to choose as soon as the spatial stimulus was presented. When they kept poking their nose into the central port over 0.5–1.0 s, it was judged as a central choice. In forced-choice trials, a spontaneous left or right choice was defined as a "hit," although failure to respond within 500 ms was defined as a "miss."

(D) Spatial choice accuracy in 3C and FC trials with graded visual contrast in session A and a fixed contrast in session B.

(E) Miss rate in 3C trials.

(F) Correct rejection rate in 3C trials.

(G) Spatial choice accuracy before and after shutter closure in FC trials.

(H) Impact of task parameters on behavioral variability using GLM fitting to left or right choice in hit and miss conditions. Model coefficients in the left panel and the ΔR^2 in the right panel are shown.

(D–H) Error bars show SEM. See also Figures S1 and S2.

enhanced-type stimulus-preferring neurons and suppressed-type stimulus-preferring neurons and the remainder as stimulus non-preferring neurons. These subpopulations consisted of heterogeneous neurons with different selectivity (Figure 2D) and different spatial distribution (Figure S3F). Importantly, both V1 and PPC neurons showed stimulus-dependent activity

Please cite this article in press as: Osako et al., Contribution of non-sensory neurons in visual cortical areas to visually guided decisions in the rat, Current Biology (2021), https://doi.org/10.1016/j.cub.2021.03.099

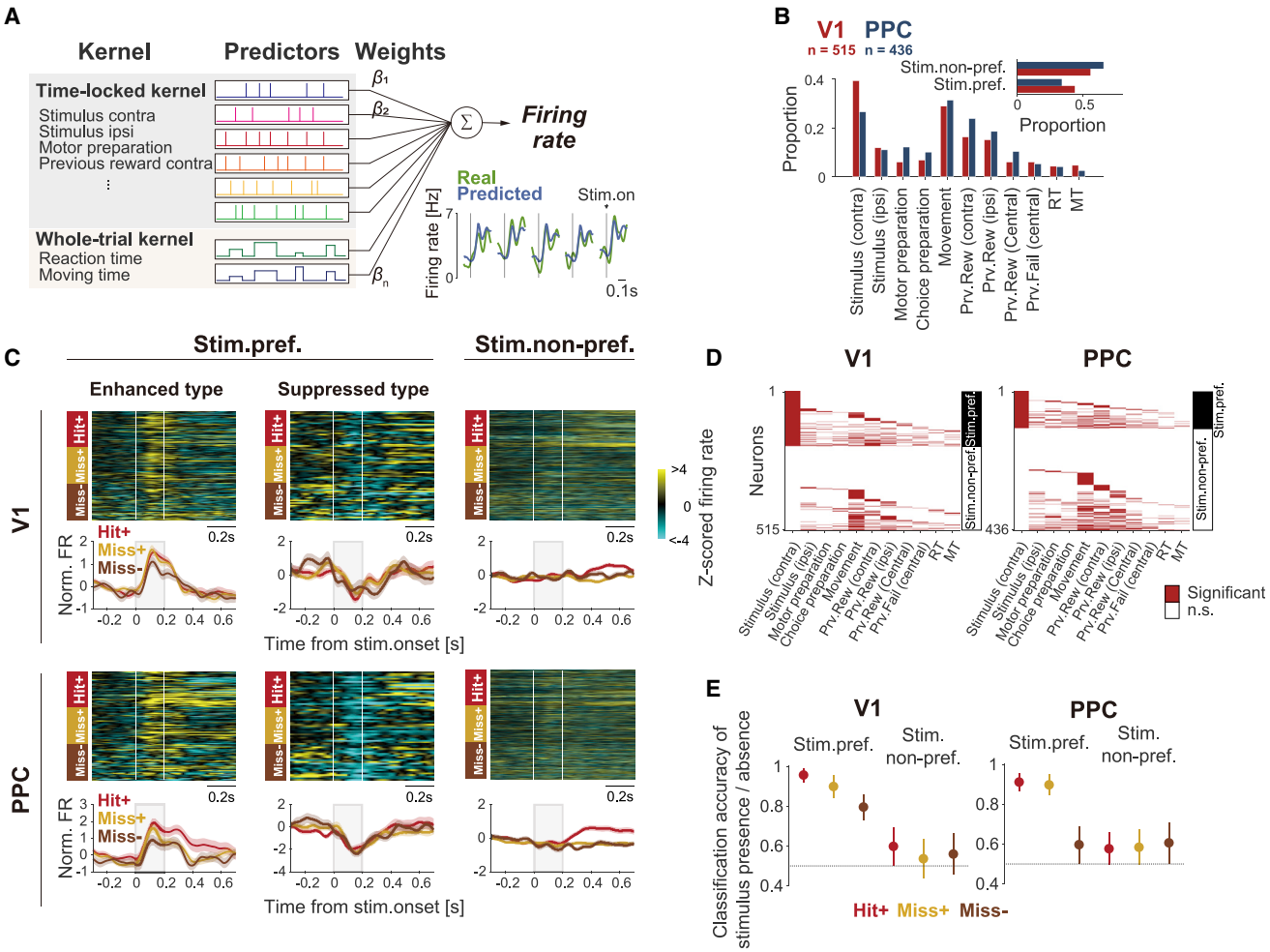

Figure 2. Quantification of neuronal responses to the task and behavioral variables in V1 and PPC neurons

(A) Schematic of the encoding model fitted to the neuronal responses to the task and behavioral variables (STAR Methods). Inset: real (green) and predicted (blue) firing rates in each cross-validated dataset are shown. Each vertical line indicates stimulus onset timing.

(B) Fraction of neurons encoding each task and behavioral variable in V1 (red) and PPC (blue). Inset: fraction of stimulus-preferring and non-preferring neurons in V1 and PPC is shown.

(C) Trial-averaged neuronal activity for each choice outcome in enhanced-type stimulus-preferring neurons (128 V1/74 PPC neurons), suppressed-type stimulus-preferring neurons (75 V1/42 PPC neurons), and stimulus non-preferring neurons (312 V1/320 PPC neurons). Firing rates of all neurons were *Z* scored and sorted by max peak latency in Hit+ trials. Shaded area shows SEM.

(D) Preferences of each neuron in V1 and PPC for task and behavioral variables (ordered within stimulus-preferring and non-preferring neurons).

(E) Classification accuracy of predicting the presence of a contralateral stimulus versus the absence of a stimulus in each choice outcome in stimulus-preferring and non-preferring population in V1 (top) and PPC (bottom). Error bars show standard deviation (SD).

See also Figure S3.

(enhanced and suppressed from pre-stimulus baseline), regardless of choice types (Figures 2C and S3D). Furthermore, the stimulus non-preferring neurons in both V1 and PPC did not show apparent differences in the average temporal dynamics among choice types until 0.2 s after stimulus presentation, where behavioral responses occurred (Figure 2C).

To further clarify whether the presence of visual information in V1 and PPC is important for hit and miss behaviors, we conducted a population-decoding analysis of the stimulus (presence or absence). We found that the stimulus-preferring population decoded stimulus presence near perfectly in the Hit+ and Miss+ trials (Figure 2E), demonstrating the robust presence of visual information both in the Miss+ and Hit+ trials. This also indicated that the stimulus period's activity was evoked by a visual stimulus, but not by stimulus expectations. We also confirmed that the stimulus non-preferring population could not predict the stimulus presence or absence even as an ensembled activity (Figures 2E and S3G). Furthermore, the classification accuracy for the Miss− trials was relatively high (~80%) in V1 but was at chance level in PPC, indicating that the visual information in PPC was not as robust as V1 in the Miss− trials. These results indicate that, in contrast to the Miss− trials, the lack of go responses in the Miss+ trials is not explained by the robustness of visual information in the visual cortex.

Please cite this article in press as: Osako et al., Contribution of non-sensory neurons in visual cortical areas to visually guided decisions in the rat, Current Biology (2021), https://doi.org/10.1016/j.cub.2021.03.099

CellPress
OPEN ACCESS

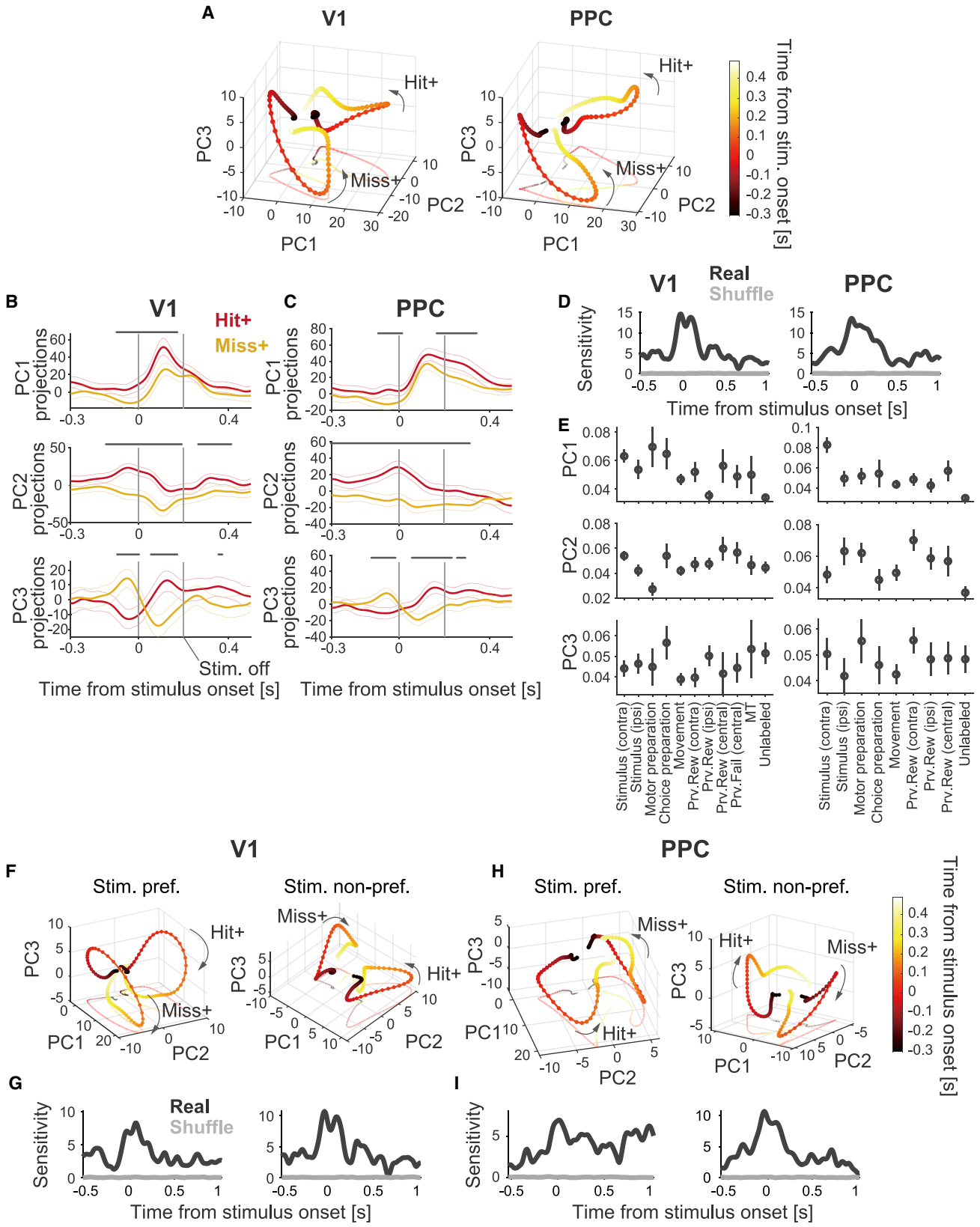

(legend on next page)

Please cite this article in press as: Osako et al., Contribution of non-sensory neurons in visual cortical areas to visually guided decisions in the rat, Current Biology (2021), https://doi.org/10.1016/j.cub.2021.03.099

Significant contributions of non-sensory neurons in V1 and PPC for separating different choice types as population activity

So far, we found no significant differences in neural activities in the Hit+ and Miss+ trials. Next, we wanted to address whether neuronal population states differentiate choice types (hereafter only referred to as Hit+ and Miss+ trials). To this end, principal component analysis (PCA) was applied to a population data consisting of trial-averaged choice-type neuronal activities ranging from −0.1 to 0.15 s after stimulus onset (see STAR Methods for details). The PCA finds the axes optimized to capture the variance of neuronal activity across choice types and time. We identified three dimensions that captured 73% of the total variance for the whole population in both V1 and PPC (Figure S4A). The reconstructed population activities from those three PCs have distinct dynamics between the Hit+ and Miss+ trials in V1 and PPC (3D plots in Figure 3A and individual PCs in Figures 3B, 3C, and S4B). We found a significant separation between choice types in the analysis window in both V1 and PPC (Figures 3D and S4C), suggesting that separation of the Hit+ and Miss+ responses is the result of the coordinated activity of many neurons. The difference of neuronal activities between the Hit+ and Miss+ trials up to 0.15 s after stimulus onset is not likely to be related to behavioral differences between Hit+ and Miss+ conditions because trials with reaction time <0.2 s were not included in the analysis (STAR Methods). On the other hand, the activity difference between Hit+ and Miss+ trials before 0.15 s after stimulus onset should reflect the difference in internal states for driving spontaneous choices in response to visual stimuli, given that rats can elicit correct spatial choices in both choice types.

Interestingly, V1 and PPC population activities shared similar PCs that may reflect neural activities to different task events and background fluctuations. For instance, PC1 shows distinct dynamics peaking around 100 ms after the onset of visual stimuli (Figures 3B and 3C). In both V1 and PPC, PC1 discriminated Hit+ and Miss+, although the time course of this effect's significance varied slightly between the two brain regions. PC2 sustained the separation of choice type information robustly before stimulus onset (Figures 3B and 3C). PC3 (Figures 3B and 3C) and others (Figure S4B) show oscillatory-like components with different frequencies, in which the phase separates choice types, suggesting a relative timing of global fluctuations across V1 and PPC to stimulus onset provides a significant influence on choice types. However, none of these components are dominated by neurons with particular selectivity (Figure 3E), except for the PC1 for PPC, dominated by stimulus-preferring neurons. In both V1 and PPC, we further confirmed a robust separative population-level activity between choice types in the stimulus non-preferring population in V1 and PPC (Figures 3F, 3H, S4A, and S4B). Other than the presence of visual-response-like components in stimulus-preferring populations, major PCs were qualitatively similar between stimulus-preferring and stimulus non-preferring populations (Figure S4B). These results indicate that Hit+ and Miss+ responses are mediated by multiple processing levels from a variety of neurons, including stimulus non-preferring neurons.

Decomposing population dynamics showed distinct state dynamics across choice types

The results above suggest the importance of non-sensory activities for separating choice types, but the association between the different task events and the population-level components is not clear. In particular, though we identified PC1 as a visual-response-like component in both V1 and PPC, it is still unclear whether other components are orthogonal to the visual-stimulus-evoked activity because the PC1 is a mixture of various neurons, including stimulus non-preferring neurons (Figure 3E), and may contain the non-stimulus factors (e.g., brain state). To further distinguish the source of non-sensory activities, we generated a neural state space spanned by orthogonalized axes that capture the population activities related to stimulus presence, internal states, decisions, and movement (Figure 4A; STAR Methods). We defined a "stimulus axis" by computing the maximally separated activity between stimulus-present and stimulus-absent trials during stimulus window (0–0.15 s from stimulus onset), a "state axis" of activity by computing the maximally separated activities between the Hit+ and Miss+ trials during the pre-stimulus window (−0.5 to 0 s from stimulus onset), a "decision axis" of activity by computing the maximally separated activities between the Hit+ and Miss+ trials during the stimulus window (0–0.15 s from stimulus onset), and a "movement axis" by computing the maximally separated activity between the Hit+ and Miss+ trials during movement window (0.3–0.5 s from stimulus onset; Figures 4B and S2). Though the selection of the analysis windows is arbitrary, we wanted to address whether and how distinct population dynamics associated with different events can separate choice types beyond the analysis window. We projected the population activities from the Hit+ and Miss+ trials onto each axis, which captured 25%/21%, 66%/51%, 16%/15%, and 26%/30% explained variance in the state, movement, stimulus, and decision axes in V1 and PPC, respectively (Figure 4C). We validated the separations of projections between the Hit+ and Miss+ trials using independent trials

Figure 3. Pre-stimulus population dynamics and stimulus subspaces in V1 and PPC

(A) Population responses of the whole population projected onto three dimensions of the analysis window (−0.1 to 0.15 s from stimulus onset) in V1 and PPC. Each color corresponds to time relative to stimulus onset.

(B and C) Mean projection of neural activity onto each principal component. Each plot is shown as a mean ± 95% confidence interval. Gray lines above each projection are significantly different across choice types.

(D) Sensitivity index (d') across choice types in the different time windows for V1 and PPC. The black line indicates real data and the thin line shuffled data.

(E) Absolute weight value in each PC shown as mean ± SEM.

(F and H) Population dynamics of stimulus-preferring and non-preferring population projected onto three dimensions of the analysis window (−0.1 to 0.15 s from stimulus onset) in V1 and PPC.

(G and I) Same as in (D) but calculated from stimulus-preferring and non-preferring populations.

See also Figure S4.

Please cite this article in press as: Osako et al., Contribution of non-sensory neurons in visual cortical areas to visually guided decisions in the rat, Current Biology (2021), https://doi.org/10.1016/j.cub.2021.03.099

CellPress
OPEN ACCESS

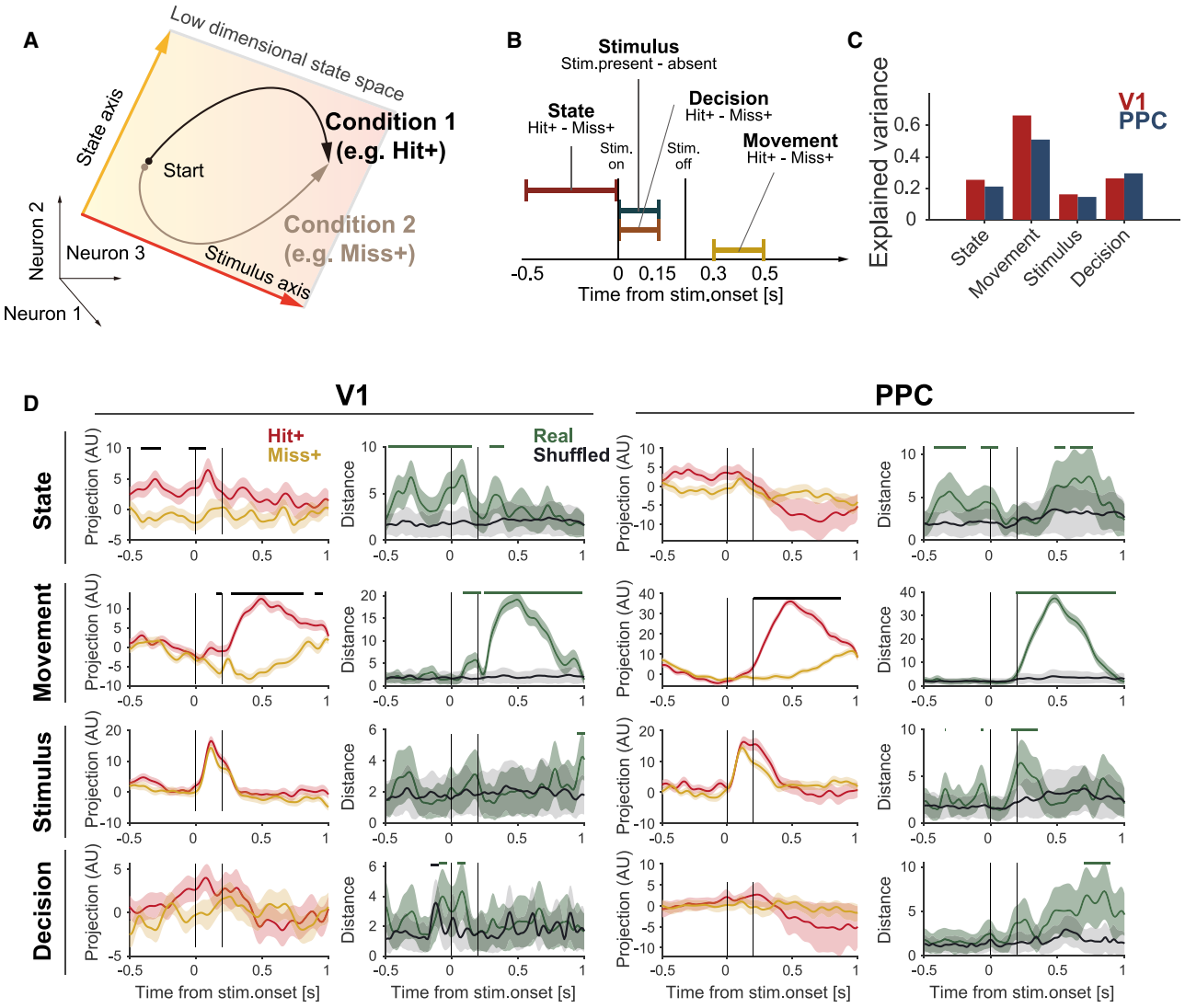

Figure 4. State dynamics regulation in V1 and PPC

(A) Population dynamics encode the two task-related variables (e.g., state and stimulus) within the two-dimensional neuronal subspace.

(B) Schematic of the definition of state, movement, stimulus, and cue-related modes. The stimulus mode was computed from stimulus presence or absence trials, and the other modes from Hit+ and Miss+ trials in each task epoch.

(C) Explained variance of each neuronal mode in original population dynamics in V1 and PPC. Note that the sign of the projections is arbitrary. The distance of projections is shown for comparison between V1 and PPC.

(D) Neuronal projections in each mode individually in V1 and PPC. Right panels in each V1 and PPC show the distance between projections in Hit+ and Miss+ trials. Shaded area shows the SD.

See also Figure S4.

from train sets (STAR Methods; $p < 0.05$; Figure 4D). We found that the population activities projected onto the pre-stimulus state axis segregated choice types as sustained dynamics beyond stimulus onset in both V1 and PPC, whereas those projected onto the decision axis showed only minor differences. On the other hand, the population activities projected onto the movement axis were largely contained within movement epoch (0.3 s after stimulus onset) without affecting stimulus epoch. Finally, we found that, consistent with decoding analysis, the stimulus-evoked population activities did not segregate choice types, at least before movement onset (<0.2 s; Figure 2E). As expected, control analysis with randomly generated data did not show such robust and unique population dynamics (Figure S4D). These results suggest distinct population dynamics orthogonally embedded to stimulus-evoked activities for separating choice types in both V1 and PPC.

The population representation of choice types is distributed across heterogeneous individual neurons

The analysis so far revealed that choice types can be discriminated with trial-averaged neuronal dynamics, but we wanted to examine whether that was the case on a single-trial basis. To

Please cite this article in press as: Osako et al., Contribution of non-sensory neurons in visual cortical areas to visually guided decisions in the rat, Current Biology (2021), https://doi.org/10.1016/j.cub.2021.03.099

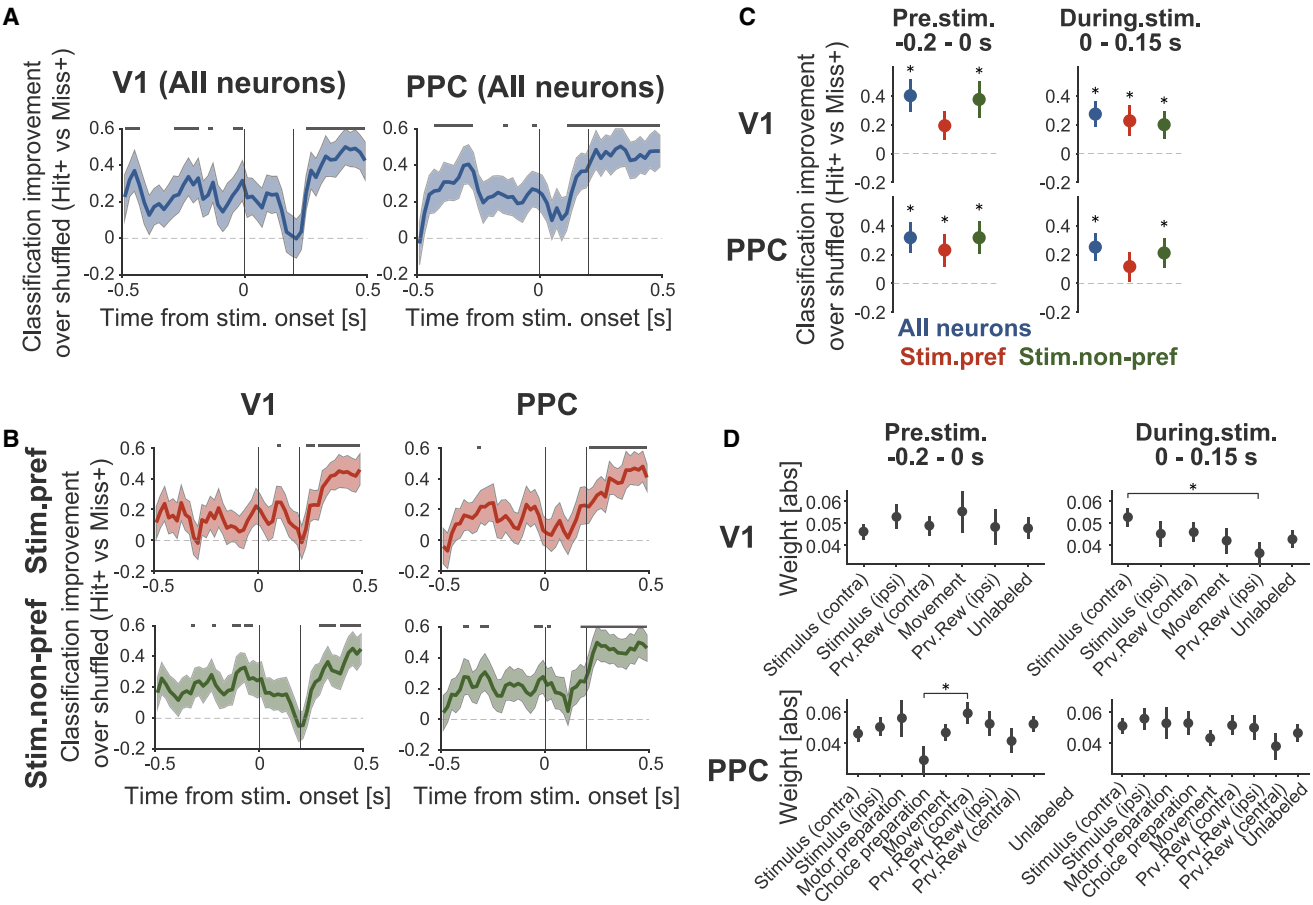

Figure 5. Predictability of distinct choice type in V1 and PPC

(A) Classification improvement (real − shuffled classification accuracy) of classifiers trained by all neurons in V1 (left) and PPC (right) in each time bin. The classifiers were independently trained in each time bin. Shaded area shows SD.

(B) Same as in (A), but each classifier trained by stimulus-preferring (left) or non-preferring neurons (right) in V1 (top) and PPC (bottom).

(C) Classification improvement in pre-stimulus epoch (−0.2 to 0 s from stimulus onset) and during stimulus (0–0.15 s from stimulus onset) for each population type. Error bars show SD. *$p < 0.05$; mean − 2SD > 0.

(D) Absolute weight value for different neurons types in classifiers trained on all neurons for each epoch. Neuron types were defined based on GLM analysis as depicted in Figures 2B and 2D except that the non-sensory neurons (e.g., prev. outcome, movement, etc.) here did not include stimulus neurons (ipsi and contra). Only neuron types with >5% of the total number of neurons are displayed. Data represent mean ± SEM. *$p < 0.05$; one-way ANOVA followed by post hoc LSD tests.

See also Figure S5.

this end, we applied a linear support vector machine (SVM) algorithm to predict the choice types (Hit+ and Miss+) of trials at each time point in V1 and PPC populations (Figure 5A). Compared with trial-label-shuffled control, we found significant improvements in the Hit+ and Miss+ classification at the time points during pre-stimulus, stimulus, and post-stimulus epochs. Note that the classification improvement in post-stimulus epoch (0.2–0.5 s from stimulus onset) simply reflects differences in behavior between the Hit+ and Miss+ trials (Figures 1C and S2). Next, we performed the same analysis dividing the population into stimulus-preferring and non-preferring neuronal subpopulations in V1 and PPC (Figure 5B). Improved classification in the pre-stimulus period was observed in the non-preferring population in both V1 and PPC and stimulus-preferring neurons in PPC (Figures 5B and 5C). The non-preferring population showed a significant classification improvement in both epochs in V1 and PPC (Figure 5C), whereas the stimulus-preferring population did not show a robust improved classification during stimulus epoch in the PPC. These results confirmed the robust contributions of the non-preferring population for separating choice types even on a trial basis throughout different time points prior to movement. Analysis of single neuronal contributions to the population decoder suggests widely distributed contributions of different neuron types in separating choice types during both pre-stimulus and stimulus epochs (Figure 5D). However, we also found biased contributions of neuron types depending on task epochs and areas: in the pre-stimulus epoch, the previous contralateral-reward-preferring neurons significantly contributed to choice-type coding compared to the stimulus-preferring neurons in PPC (Figure 5D; $p < 0.05$; one-way ANOVA followed by least significant difference [LSD] multiple comparisons), although, during-stimulus epoch, stimulus-preferring neurons contributed to

Please cite this article in press as: Osako et al., Contribution of non-sensory neurons in visual cortical areas to visually guided decisions in the rat, Current Biology (2021), https://doi.org/10.1016/j.cub.2021.03.099

the coding compared with the previous ipsi-reward-preferring neurons in V1 (Figure 5D; $p < 0.05$; one-way ANOVA followed by LSD multiple comparisons).

We next asked whether the population computation for choice types dynamically changed or was stable over time. A cross-temporal classification analysis was performed to probe the stability of neuronal population computation (Figures S5A and S5B). As expected, the highest stability of classifiers was found around the time where the behavioral differences between Hit+ and Miss+ trials occurred (0.2–0.5 s after stimulus onset). Other than that, pre-stimulus classifiers were relatively stable at least until 0.1 s from stimulus onset in all neurons and stimulus non-preferring neurons in PPC, whereas the stimulus-preferring population showed less stability in the cross-temporal classification (Figure S5B). To estimate the stability of neuron contributions for the classification of choice types across time, we calculated Pearson's correlation coefficients of neuronal weights of pairs of classifiers at different times (Figures S5C and S5D). If the population computation is similar across time, the correlation coefficients will be tolerant to decaying. For a comparison between whole populations in V1 and PPC (Figure S5D, top; $p < 0.01$; Kruskal-Wallis test), V1 was relatively dynamic compared to PPC. Such a dynamic population computation was, in particular, evident in both stimulus-preferring and non-preferring neurons in V1 (Figure S5D, below), whereas the stability was relatively higher in non-preferring populations in the PPC than elsewhere (Figure S5D, below; $p < 0.05$; the Kruskal-Wallis test followed by post hoc Tukey's tests for comparison). Together, these results suggest that choice information was stable over time, especially in stimulus non-preferring neurons, although population computation is dynamic, especially in V1.

V1 noise correlation increased in forced detection performance before and after stimulus presentation

Thus far, our results demonstrate that non-preferring neurons encode choice types in V1 and PPC. However, in these analyses, we used a "pseudo-population" that combined neuronal activity recorded in different trials. Therefore, our analysis did not consider the correlation structure of pairs of simultaneously recorded neurons within each trial (i.e., noise correlation). If the noise is closer to random across neurons (low noise correlation), information coding can be more reliable and efficient[44] (but see Moreno-Bote et al.[45]). We first examined classification accuracy in each session using a simultaneously recorded population. Both V1 and PPC populations showed a significantly higher classification than shuffled data (Figure 6A; $p < 0.001$ in V1 and PPC). Next, we compared classification accuracy with a de-correlated population where each neuron in the same session was randomly selected from different trials within the same choice type (STAR Methods). Thus, the de-correlated population maintains the signal correlation while removing the noise correlation. Both V1 and PPC populations had significantly decreased classification accuracy in the de-correlated population (Figure 6B), indicating that the correlation structure was crucial for population computation.

To investigate the correlation structure in choice types, we calculated pairwise noise correlations separately for Hit+ and Miss+ conditions at each time bin (STAR Methods; Figure 6C). We found that noise correlation in Miss+ trials increased in pre-stimulus epoch and during stimulus epoch compared to Hit+ trials in V1 neuron pairs, although PPC neuron pairs did not differ in choice types (Figure 6C). Such a difference in noise correlation was mostly apparent in neuron pairs among regular-spiking neurons (Figure S6C). We next asked whether reduced noise correlation is associated with pairs of neuronal types (i.e., stimulus-preferring and non-preferring neurons). The increased noise correlation in Miss+ trials was most evident in pairwise interactions between stimulus preferring and non-preferring neurons and non-preferring and non-preferring neurons, especially during pre-stimulus epoch (Figure 6D). These results suggest that neuronal coupling associated with stimulus non-preferring neurons in V1 plays an important role in separating choice types.

DISCUSSION

It is widely believed that the fidelity of visual responses in sensory neurons explains the trial-by-trial variance of visual detection performance. Our results demonstrated significant contributions of non-sensory neurons in V1 and PPC to reliable visual detection performance. The near-threshold stimuli used in our task induced trial-by-trial variability in visual detection performance, and we further classified those trials with identical stimuli into three choice types, which were not differentiated in previous studies. Surprisingly, the Hit+ and Miss+ trials showed no differences in population encoding of stimulus as well as mean temporal dynamics (Figures 2C and S3D, right). Instead, we found multiple lines of evidence for population-level computation contributing to the optimal behavioral responses to visual stimuli (Hit+ and Miss+) in V1 and PPC. First, we found a specific divergence between choice types at multiple levels of population activity, particularly with the robust contribution from stimulus non-preferring neurons in both V1 and PPC, which is orthogonally embedded to stimulus response dynamics (Figures 3 and 4). Second, during pre-stimulus and stimulus epochs, the choice types were decoded on a single-trial basis with contributions of a variety of neurons with different selectivity in both V1 and PPC (Figure 5). Third, V1 neuron pairs, but not PPC, showed increased noise correlation in the Miss+ trials compared to the Hit+ trials before and during visual stimulus presentation, which was most evident in pairwise interactions between non-preferring neurons and others (Figures 6C and 6D).

It has been postulated that stochastic behavioral responses to identical sensory stimuli are generated by fluctuations of background neuronal ensembles preceding external inputs.[46] A recent study further demonstrated that a global slow oscillation correlates with the level of task engagement measured by miss rates.[47] Our unsupervised analysis revealed at least three major distinct population dynamics in V1 and PPC, respectively (Figure 3). First, we found temporal dynamics coinciding with the visual response peak in both V1 and PPC. Second, we found sustained dynamics, which significantly contributed to separating the choice types well before stimulus onset (Figures 3 and S4B). The choice type was orthogonally represented to the visual response dynamics with involvement of non-sensory neurons (Figures 3 and 4). Third, we found that oscillatory components, which were prominent in both stimulus-preferring and non-preferring neurons of both V1 and PPC, were significant factors

Please cite this article in press as: Osako et al., Contribution of non-sensory neurons in visual cortical areas to visually guided decisions in the rat, Current Biology (2021), https://doi.org/10.1016/j.cub.2021.03.099

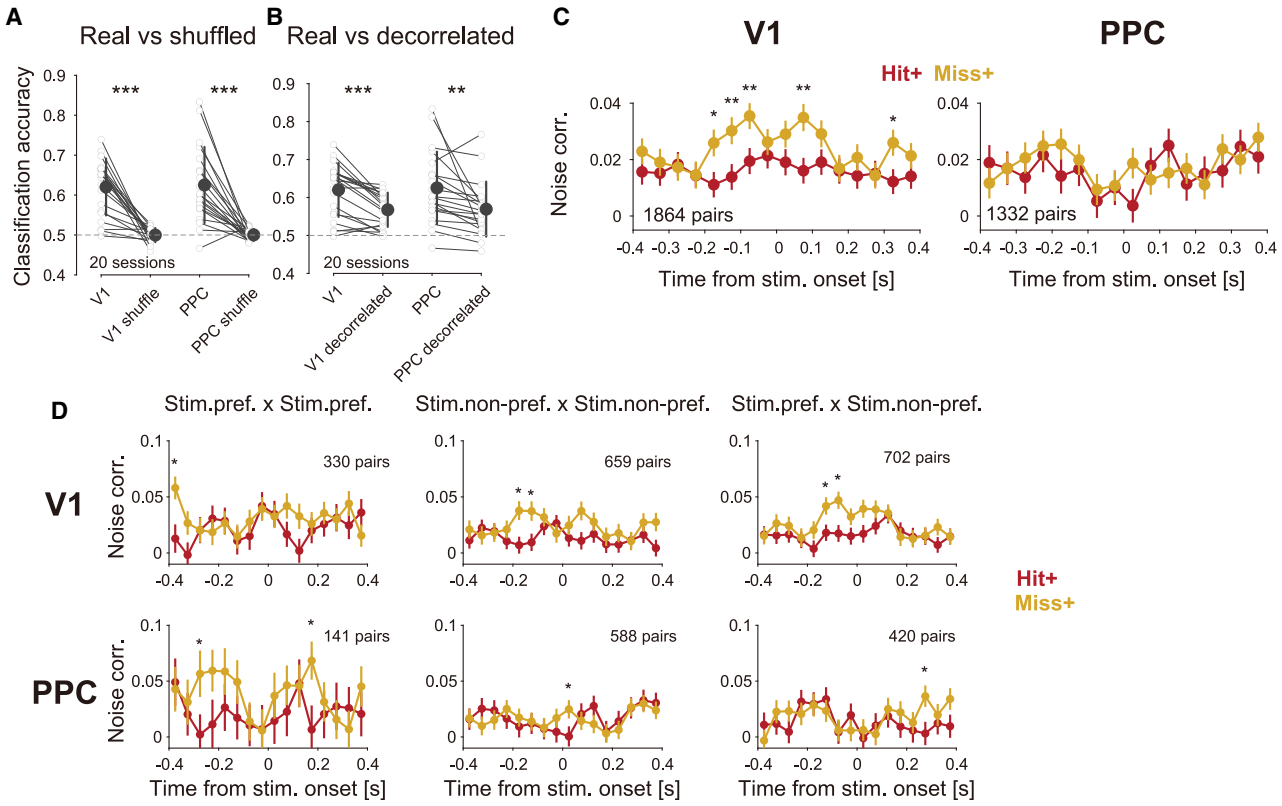

Figure 6. Noise correlation in Miss+ trials increased around stimulus presentation in V1

(A) Classification accuracy for real and shuffled populations in each session in V1 and PPC. ***p < 0.001 in V1; paired t test.

(B) Classification accuracy for the real and de-correlated population in each session in V1 and PPC. **p < 0.01; ***p < 0.001; paired t test.

(C) Mean noise correlation in each time epoch in V1 and PPC. The error bars show SEM. *p < 0.05; **p < 0.01; t test.

(D) Mean noise correlation in each time epoch with different neuron type combinations in V1 and PC. *p < 0.05; paired t test.

See also Figure S6.

to differentiate choice types (Figures 3 and S4B). Accordingly, we have two non-exclusive hypotheses on how stimulus non-preferring neurons can influence this process.

First, the extent of local interactions between stimulus non-preferring neurons and stimulus-preferring neurons may determine the deviation of choice between optimal (hit) and conservative (miss). Although our state space analyses (Figures 3 and 4) suggest that visual responses within stimulus-preferring population are orthogonally represented with the state signals, the mixed population of stimulus-preferring and non-preferring neurons in V1 represented visual responses with coherent modulation by state signals (PC1; Figure 3), suggesting significant interactions between stimulus-preferring and non-preferring neurons on a trial-by-trial basis that affect hit or miss behavior. Supporting this hypothesis, we found that the correlation structure among simultaneously recorded neurons around the stimulus presentation time can contribute to the separation of choice types (Figure 6B). Furthermore, we found an increased noise correlation in the Miss+ trials between stimulus non-preferring and others (Figures 6C and 6D), suggesting that the relative timing of the visual stimulus with respect to the ongoing interactions among these neurons affects visual processing, resulting in biased decisions (i.e., Miss+ trials). Thus, we suggest proper interaction between stimulus-preferring and non-preferring neurons on a trial-by-trial basis underlies the optimal exploitation of visual information for behavior. However, we note that increased noise correlation is not necessarily harmful for information coding.[45,48] Future studies will address whether and how downstream cortical areas exploit the integrated information for behavior.

Second, global oscillatory activities, including stimulus non-preferring neurons, support visual information transmission to downstream cortical areas. We observed various subtle oscillatory components, where the phase separated the choice types relative to the stimulus onset, suggesting that visual inputs can be efficiently exploited for behavior when the ongoing fluctuation is in a particular phase. The finding is consistent with previous studies that proposed that sensory information is gated by ongoing neural activities.[46,49–51] However, we did not obtain direct evidence that local field potential (LFP) corresponds to those spike oscillations. It is possible that LFP oscillation and spike oscillation from a particular subpopulation can be controlled differently. For instance, a recent study suggested that non-sensory-tuned fast-spiking neurons originate cortical rhythmicity, resulting in the direct influence on sensory information coding in the primary somatosensory cortex.[51] Future work

will address the possibility that supports the local network mechanism and directionality of information flow between stimulus-preferring and non-preferring neuronal coupling.

The relatively weak contribution of visually evoked activities in V1 and PPC population coding could be a unique feature of our task design because animals had a third option, of which experienced reward value may suppress peripheral choices, even when the animals recognize the stimuli. It should be noted that ignoring the presence of stimuli is never rewarded in our task and, thus, is clearly suboptimal bias behavior. In addition, our data show that rewards in the previous trials only partially (about 10%) explain the behavioral variance in hit or miss choices (Figure S1F) as well as the variance of population neural coding in V1 and PPC (Figure 5D). Therefore, we conclude that the previous rewards cannot solely explain the recruitment of non-sensory neurons in V1 and PPC. On the other hand, it is possible that task-irrelevant movements during task performance could have affected hit responses due to suboptimal head and body positions.[52,53] However, such behavioral misalignment does not explain the increased noise correlation in V1. This suggests that, at least, the accurate performance in hit trials is due to an intrinsic population-level mechanism that can be related to sensory-motor transformation during the task,[40] while highlighting the non-trivial contribution of non-sensory neurons in the process. Although previous studies indicated the significant contributions of non-sensory neurons to perceptual decision making,[28–30,54] most of them employed sensory categorization tasks in the forced-choice paradigm, which unavoidably suffers from stimulus uncertainty causing subjective biases due to value-based decisions. Our data support and extend these findings by showing that, even in the simplest sensory detection task, lacking inherent stimulus uncertainty and being less contaminated by value-based decisions, non-sensory neurons in V1 and PPC play a significant role in sensory decisions at the population level.

STAR★METHODS

Detailed methods are provided in the online version of this paper and include the following:

- KEY RESOURCES TABLE
- RESOURCE AVAILABILITY
  - Lead contact
  - Materials availability
  - Data and code availability
- EXPERIMENTAL MODEL AND SUBJECT DETAILS
  - Subjects
  - Surgery
  - Histology
- METHOD DETAILS
  - Behavioral apparatus
  - Visual cue detection task
  - Electrophysiological recordings
  - Spike sorting and screening criteria of units
  - Behavioral data analysis
- QUANTIFICATION AND STATISTICAL ANALYSIS
  - Time-locked kernel regression and visual sensitivity
  - Spike train analysis
  - Statistics
  - State-space analysis
  - State space analysis at each task and behavioral axis
  - Classification (decoding) analysis
  - Stability (cross-temporal classification analysis)
  - Noise correlation
  - Cell-type classification

SUPPLEMENTAL INFORMATION

Supplemental information can be found online at https://doi.org/10.1016/j.cub.2021.03.099.

ACKNOWLEDGMENTS

We would like to thank the members of the Laboratory of Neural Information at Doshisha University for helpful discussions. This research was supported by the JSPS KAKENHI grant numbers 19J21544 (to Y.O.), 20H00109 and 20H05020 (to Y.S.), 19J12634 (to T.O.), and 16K18380, 19H05028, and 19K06948 (to J.H.).

AUTHOR CONTRIBUTIONS

Y.O., T.O., Y.S., and J.H. designed the experiments. Y.O. performed the experiments and analyzed the data. T.O., Y.T., and K.S. analyzed the data. H.M., Y.S., and J.H. supervised the project. All authors contributed to writing the manuscript.

DECLARATION OF INTERESTS

The authors declare no competing interests.

Received: November 4, 2020
Revised: March 15, 2021
Accepted: March 31, 2021
Published: April 22, 2021

REFERENCES

1. Osako, Y., Sakurai, Y., and Hirokawa, J. (2018). Subjective decision threshold for accurate visual detection performance in rats. Sci. Rep. *8*, 9357.
2. van Vugt, B., Dagnino, B., Vartak, D., Safaai, H., Panzeri, S., Dehaene, S., and Roelfsema, P.R. (2018). The threshold for conscious report: signal loss and response bias in visual and frontal cortex. Science *360*, 537–542.
3. Merikle, P.M., Smilek, D., and Eastwood, J.D. (2001). Perception without awareness: perspectives from cognitive psychology. Cognition *79*, 115–134.
4. Kolb, F.C., and Braun, J. (1995). Blindsight in normal observers. Nature *377*, 336–338.
5. Osborne, L.C., Hohl, S.S., Bialek, W., and Lisberger, S.G. (2007). Time course of precision in smooth-pursuit eye movements of monkeys. J. Neurosci. *27*, 2987–2998.
6. Parker, A.J., and Newsome, W.T. (1998). Sense and the single neuron: probing the physiology of perception. Annu. Rev. Neurosci. *21*, 227–277.
7. Tolhurst, D.J., Movshon, J.A., and Dean, A.F. (1983). The statistical reliability of signals in single neurons in cat and monkey visual cortex. Vision Res. *23*, 775–785.
8. Busse, L., Ayaz, A., Dhruv, N.T., Katzner, S., Saleem, A.B., Schölvinck, M.L., Zaharia, A.D., and Carandini, M. (2011). The detection of visual contrast in the behaving mouse. J. Neurosci. *31*, 11351–11361.
9. Smallwood, J., and Schooler, J.W. (2006). The restless mind. Psychol. Bull. *132*, 946–958.

10. Aston-Jones, G., and Cohen, J.D.A.N. (2005). An integrative theory of locus coeruleus-norepinephrine function: adaptive gain and optimal performance. Annu. Rev. Neurosci. *28*, 403–450.

11. Critchley, H.D., and Rolls, E.T. (1996). Hunger and satiety modify the responses of olfactory and visual neurons in the primate orbitofrontal cortex. J. Neurophysiol. *75*, 1673–1686.

12. Schriver, B.J., Bagdasarov, S., and Wang, Q. (2018). Pupil-linked arousal modulates behavior in rats performing a whisker deflection direction discrimination task. J. Neurophysiol. *120*, 1655–1670.

13. Harris, K.D., and Thiele, A. (2011). Cortical state and attention. Nat. Rev. Neurosci. *12*, 509–523.

14. Monto, S., Palva, S., Voipio, J., and Palva, J.M. (2008). Very slow EEG fluctuations predict the dynamics of stimulus detection and oscillation amplitudes in humans. J. Neurosci. *28*, 8268–8272.

15. Niell, C.M., and Stryker, M.P. (2010). Modulation of visual responses by behavioral state in mouse visual cortex. Neuron *65*, 472–479.

16. Jacobs, E.A.K., Steinmetz, N.A., Peters, A.J., Carandini, M., and Harris, K.D. (2020). Cortical state fluctuations during sensory decision making. Curr. Biol. *30*, 4944–4955.e7.

17. Shimaoka, D., Steinmetz, N.A., Harris, K.D., and Carandini, M. (2019). The impact of bilateral ongoing activity on evoked responses in mouse cortex. eLife *8*, 1–19.

18. Lak, A., Okun, M., Moss, M.M., Gurnani, H., Farrell, K., Wells, M.J., Reddy, C.B., Kepecs, A., Harris, K.D., and Carandini, M. (2020). Dopaminergic and prefrontal basis of learning from sensory confidence and reward value. Neuron *105*, 700–711.e6.

19. Lak, A., Nomoto, K., Keramati, M., Sakagami, M., and Kepecs, A. (2017). Midbrain dopamine neurons signal belief in choice accuracy during a perceptual decision. Curr. Biol. *27*, 821–832.

20. Daw, N.D., O'Doherty, J.P., Dayan, P., Seymour, B., and Dolan, R.J. (2006). Cortical substrates for exploratory decisions in humans. Nature *441*, 876–879.

21. Gold, J.I., Law, C.T., Connolly, P., and Bennur, S. (2008). The relative influences of priors and sensory evidence on an oculomotor decision variable during perceptual learning. J. Neurophysiol. *100*, 2653–2668.

22. Akaishi, R., Umeda, K., Nagase, A., and Sakai, K. (2014). Autonomous mechanism of internal choice estimate underlies decision inertia. Neuron *81*, 195–206.

23. Fan, Y., Gold, J.I., and Ding, L. (2018). Ongoing, rational calibration of reward-driven perceptual biases. eLife *7*, 1–26.

24. Fritsche, M., Mostert, P., and de Lange, F.P. (2017). Opposite effects of recent history on perception and decision. Curr. Biol. *27*, 590–595.

25. Hirokawa, J., Vaughan, A., Masset, P., Ott, T., and Kepecs, A. (2019). Frontal cortex neuron types categorically encode single decision variables. Nature *576*, 446–451.

26. Masset, P., Ott, T., Lak, A., Hirokawa, J., and Kepecs, A. (2020). Behavior- and modality-general representation of confidence in orbitofrontal cortex. Cell *182*, 112–126.e18.

27. Hwang, E.J., Dahlen, J.E., Mukundan, M., and Komiyama, T. (2017). History-based action selection bias in posterior parietal cortex. Nat. Commun. *8*, 1242.

28. Safaai, H., von Heimendahl, M., Sorando, J.M., Diamond, M.E., and Maravall, M. (2013). Coordinated population activity underlying texture discrimination in rat barrel cortex. J. Neurosci. *33*, 5843–5855.

29. Leavitt, M.L., Pieper, F., Sachs, A.J., and Martinez-Trujillo, J.C. (2017). Correlated variability modifies working memory fidelity in primate prefrontal neuronal ensembles. Proc. Natl. Acad. Sci. USA *114*, E2494–E2503.

30. Insanally, M.N., Carcea, I., Field, R.E., Rodgers, C.C., DePasquale, B., Rajan, K., DeWeese, M.R., Albanna, B.F., and Froemke, R.C. (2019). Spike-timing-dependent ensemble encoding by non-classically responsive cortical neurons. eLife *8*, 1–31.

31. Silvanto, J., Muggleton, N., Lavie, N., and Walsh, V. (2009). The perceptual and functional consequences of parietal top-down modulation on the visual cortex. Cereb. Cortex *19*, 327–330.

32. Goard, M.J., Pho, G.N., Woodson, J., and Sur, M. (2016). Distinct roles of visual, parietal, and frontal motor cortices in memory-guided sensorimotor decisions. eLife *5*, 1–30.

33. Weiskrantz, L. (1986). Blindsight: A Case Study in its Implications (Oxford University).

34. Campion, J., Latto, R., and Smith, Y.M. (1983). Is blindsight an effect of scattered light, spared cortex, and near-threshold vision? Behav. Brain Sci. *6*, 423–448.

35. Glickfeld, L.L., Histed, M.H., and Maunsell, J.H.R. (2013). Mouse primary visual cortex is used to detect both orientation and contrast changes. J. Neurosci. *33*, 19416–19422.

36. Hwang, E.J., Link, T.D., Hu, Y.Y., Lu, S., Wang, E.H., Lilascharoen, V., Aronson, S., O'Neil, K., Lim, B.K., and Komiyama, T. (2019). Corticostriatal flow of action selection bias. Neuron *104*, 1126–1140.e6.

37. Hishida, R., Horie, M., Tsukano, H., Tohmi, M., Yoshitake, K., Meguro, R., Takebayashi, H., Yanagawa, Y., and Shibuki, K. (2019). Feedback inhibition derived from the posterior parietal cortex regulates the neural properties of the mouse visual cortex. Eur. J. Neurosci. *50*, 2970–2987.

38. Marques, T., Nguyen, J., Fioreze, G., and Petreanu, L. (2018). The functional organization of cortical feedback inputs to primary visual cortex. Nat. Neurosci. *21*, 757–764.

39. Keller, A.J., Roth, M.M., and Scanziani, M. (2020). Feedback generates a second receptive field in neurons of the visual cortex. Nature *582*, 545–549.

40. Pho, G.N., Goard, M.J., Woodson, J., Crawford, B., and Sur, M. (2018). Task-dependent representations of stimulus and choice in mouse parietal cortex. Nat. Commun. *9*, 2596.

41. Montijn, J.S., Goltstein, P.M., and Pennartz, C.M.A. (2015). Mouse V1 population correlates of visual detection rely on heterogeneity within neuronal response patterns. eLife *4*, e10163.

42. Hanks, T.D., Kopec, C.D., Brunton, B.W., Duan, C.A., Erlich, J.C., and Brody, C.D. (2015). Distinct relationships of parietal and prefrontal cortices to evidence accumulation. Nature *520*, 220–223.

43. Green, D.M., and Swets, J.A. (1966). Signal Detection Theory and Psychophysics (Wiley).

44. Rumyantsev, O.I., Lecoq, J.A., Hernandez, O., Zhang, Y., Savall, J., Chrapkiewicz, R., Li, J., Zeng, H., Ganguli, S., and Schnitzer, M.J. (2020). Fundamental bounds on the fidelity of sensory cortical coding. Nature *580*, 100–105.

45. Moreno-Bote, R., Beck, J., Kanitscheider, I., Pitkow, X., Latham, P., and Pouget, A. (2014). Information-limiting correlations. Nat. Neurosci. *17*, 1410–1417.

46. Speed, A., Del Rosario, J., Burgess, C.P., and Haider, B. (2019). Cortical state fluctuations across layers of V1 during visual spatial perception. Cell Rep. *26*, 2868–2874.e3.

47. Jacobs, E.A.K., Steinmetz, N.A., Peters, A.J., Carandini, M., and Harris, K.D. (2020). Cortical state fluctuations during sensory decision making. Curr. Biol. *30*, 4944–4955.e7.

48. Montijn, J.S., Meijer, G.T., Lansink, C.S., and Pennartz, C.M.A. (2016). Population-level neural codes are robust to single-neuron variability from a multidimensional coding perspective. Cell Rep. *16*, 2486–2498.

49. Zylberberg, J. (2018). The role of untuned neurons in sensory information coding. bioRxiv. https://doi.org/10.1101/134379.

50. Allen, W.E., Chen, M.Z., Pichamoorthy, N., Tien, R.H., Pachitariu, M., Luo, L., and Deisseroth, K. (2019). Thirst regulates motivated behavior through modulation of brainwide neural population dynamics. Science *364*, eaav3932.

51. Shin, H., and Moore, C.I. (2019). Persistent gamma spiking in SI nonsensory fast spiking cells predicts perceptual success. Neuron *103*, 1150–1163.e5.

52. Musall, S., Kaufman, M.T., Juavinett, A.L., Gluf, S., and Churchland, A.K. (2019). Single-trial neural dynamics are dominated by richly varied movements. Nat. Neurosci. *22*, 1677–1686.

53. Krumin, M., Lee, J.J., Harris, K.D., and Carandini, M. (2018). Decision and navigation in mouse parietal cortex. eLife *7*, 1–18.

54. Zuo, Y., and Diamond, M.E. (2019). Texture identification by bounded integration of sensory cortical signals. Curr. Biol. *29*, 1425–1435.e5.

55. Ohnuki, T., Osako, Y., Manabe, H., Sakurai, Y., and Hirokawa, J. (2020). Dynamic coordination of the perirhinal cortical neurons supports coherent representations between task epochs. Commun. Biol. *3*, 406.

56. Sanders, J.I., and Kepecs, A. (2014). A low-cost programmable pulse generator for physiology and behavior. Front. Neuroeng. *7*, 43.

57. Harris, K.D., Hirase, H., Leinekugel, X., Henze, D.A., and Buzsáki, G. (2001). Temporal interaction between single spikes and complex spike bursts in hippocampal pyramidal cells. Neuron *32*, 141–149.

58. Steinmetz, N.A., Zatka-Haas, P., Carandini, M., and Harris, K.D. (2019). Distributed coding of choice, action and engagement across the mouse brain. Nature *576*, 266–273.

59. Banerjee, A., Parente, G., Teutsch, J., Lewis, C., Voigt, F.F., and Helmchen, F. (2020). Value-guided remapping of sensory cortex by lateral orbitofrontal cortex. Nature *585*, 245–250.

60. Parthasarathy, A., Herikstad, R., Bong, J.H., Medina, F.S., Libedinsky, C., and Yen, S.C. (2017). Mixed selectivity morphs population codes in prefrontal cortex. Nat. Neurosci. *20*, 1770–1779.

61. Li, N., Daie, K., Svoboda, K., and Druckmann, S. (2016). Robust neuronal dynamics in premotor cortex during motor planning. Nature *532*, 459–464.

62. Mante, V., Sussillo, D., Shenoy, K.V., and Newsome, W.T. (2013). Context-dependent computation by recurrent dynamics in prefrontal cortex. Nature *503*, 78–84.

63. Najafi, F., Elsayed, G.F., Cao, R., Pnevmatikakis, E., Latham, P.E., Cunningham, J.P., and Churchland, A.K. (2020). Excitatory and inhibitory subnetworks are equally selective during decision-making and emerge simultaneously during learning. Neuron *105*, 165–179.e8.

64. Montijn, J.S., Vinck, M., and Pennartz, C.M.A. (2014). Population coding in mouse visual cortex: response reliability and dissociability of stimulus tuning and noise correlation. Front. Comput. Neurosci. *8*, 58.

Please cite this article in press as: Osako et al., Contribution of non-sensory neurons in visual cortical areas to visually guided decisions in the rat, Current Biology (2021), https://doi.org/10.1016/j.cub.2021.03.099

STAR★METHODS

KEY RESOURCES TABLE

REAGENT or RESOURCE	SOURCE	IDENTIFIER
Chemicals, peptides, and recombinant proteins		
Isoflurane	Wakenyaku, Kyoto, Japan	N/A
Dental Cement	Wakenyaku, Kyoto, Japan	Unifast 3
Deposited data		
Data deposited at Mendeley Data	This paper	https://doi.org/10.17632/wxcpcb47pv.1
Experimental models: organisms/strains		
Long-Evans Hooded Rat	Shimizu Laboratory Supplies, Kyoto, Japan	N/A
Software and algorithms		
MATLAB	MathWorks	Version 2020a
Glmnet in MATLAB	Qian, J., Hastie, T., Friedman, J., Tibshirani, R., and Simon, N.	https://web.stanford.edu/~hastie/glmnet_matlab/
Time-locked kernel regression analysis	This paper	https://github.com/YumaOsako/EncodingModel
Spike sorting	MClust	http://redishlab.neuroscience.umn.edu/MClust/MClust.html
PulsePal and Bpod	J. Sanders and A. Kepecs.	https://www.sanworks.io/index.php
Arduino	N/A	https://www.arduino.cc/
Other		
Open Ephys Acquisition Board	Open Ephys	https://open-ephys.org/acq-board
3D printing (for microdrive)	DMM.make	https://make.dmm.com/print/

RESOURCE AVAILABILITY

Lead contact

Further information and requests for resources should be directed to the Lead Contact, Yuma Osako (dddb1003@mail4.doshisha.ac.jp) or Junya Hirokawa (jhirokaw@mail.doshisha.ac.jp).

Materials availability

This study did not generate new unique reagents.

Data and code availability

The electrophysiological data during behavioral task generated in this study have been deposited on Mendeley Data: https://doi.org/10.17632/wxcpcb47pv.1. The code for the time-locked kernel regression is available on GitHub (https://github.com/YumaOsako/EncodingModel). All other code is available upon reasonable request.

EXPERIMENTAL MODEL AND SUBJECT DETAILS

Subjects

Seven male Long-Evans rats (Shimizu Laboratory Supplies, Kyoto, Japan) weighing 200-268 g at the beginning of training were individually housed and maintained on a laboratory light/dark cycle (lights on 8:00 A.M. to 9:00 P.M.). Rats were placed on water restriction with *ad libitum* access to food. The animals were maintained at 80% of their baseline weight throughout the experiments. All experiments were implemented in accordance with the guidelines for the care and use of laboratory animals provided by the Animal Research Committee of Doshisha University.

Surgery

Rats were anesthetized with 2.5% isoflurane before surgery, and anesthesia maintained throughout surgical procedures. We monitored body movements and hind leg reflex and adjusted the depth of anesthesia as needed. An eye ointment was used to keep the eyes moistened throughout the surgery. Subcutaneous scalp injection of a lidocaine 1% solution provided local anesthesia before

Please cite this article in press as: Osako et al., Contribution of non-sensory neurons in visual cortical areas to visually guided decisions in the rat, Current Biology (2021), https://doi.org/10.1016/j.cub.2021.03.099

the incision. A craniotomy was performed over the anterior part of the right V1 (AP −6.36 to −7.32 mm, ML 3.2 mm relative to the bregma, 0.2 to 0.4 mm below the brain surface), and right PPC (AP −3.8 mm, ML: 2.5 mm relative to the bregma, 0.2 to 0.4 mm below the brain surface), and a custom-designed electrode was vertically implanted using a stereotactic manipulator. A stainless-steel screw was placed over the cerebellum and served as ground during recordings. The mean response of all electrodes was used as a reference. During a week of postsurgical recovery, we gradually lowered the tetrodes to detect unit activities in the V1 and PPC. Electrode placement was estimated based on depth and was histologically confirmed at the end of experiments.

Histology

Once the experiments were completed, the rats were deeply anesthetized with sodium pentobarbital and then transcardially perfused with phosphate-buffered saline and 4% paraformaldehyde. The brains were removed and post-fixed in 4% paraformaldehyde, and 100 μm coronal brain sections were prepared to confirm the recording sites (Figure S3E).

METHOD DETAILS

Behavioral apparatus

The behavioral apparatus (Figures 1A–1C) has been previously described.[1,55] An operant chamber (O'Hara, Tokyo, Japan) with three ports in the front wall for nose-poke responses was enclosed in a soundproof box (Brain Science Idea, Osaka, Japan). Each port was equipped with an infrared sensor to detect the animals' nose-poke responses. Visual cues were presented using white light-emitting diodes (LEDs) (4000 mcd; RS Components, Yokohama, Japan) placed on the left and right walls of the operant chamber, as shown in Figure 1. Water rewards were delivered from gravity-fed reservoirs regulated by solenoid valves (The Lee Company, Westbrook, CT) through stainless tubes placed inside the central, left and right target ports. Stimulus and reward deliveries were controlled with Pulse Pal[56] and behavioral responses measured using Bpod (Sanworks, Stony Brook, NY).

Visual cue detection task

The visual cue detection task design was previously described.[1] The task consisted of randomly interleaved three-choice (3C) and forced-choice (FC) trials with equal probabilities in a session. The only difference between trial types was that in FC trials, the central port was closed with the shutter door to prevent the rat from continuing to the central nose poke (Figures 1A–1C). After a fixed 3 s inter-trial interval (ITI), the central port was illuminated by an interior LED, signaling the ready state of trial initiation. The rats initiated each trial by making nose pokes into the central port. After a 0.2−0.6 s random stimulus delay, the visual stimulus was presented from the left or right side for a duration of 0.2 s. Rats were allowed to make a choice response after the end of the stimulus delay period. Trials in which animals prematurely left the port before stimulus delay were canceled and trials re-initiated. We randomly provided one of three levels of visual brightness (difficult, medium, and easy) for each trial by modulating the voltage between 0.02−5.1 lux in session A. Difficult and easy stimuli were selected for all subjects based on the minimum and maximum LED voltage dynamic range. Medium stimuli were chosen for each subject such that the subject detected stimuli with medium accuracy between easy and difficult stimuli in forced-choice trials. The probabilities for left, right, or no visual stimulus were equal (33% per condition) in 3C and FC trials. The reward was given if rats chose the same side where the visual stimuli were emitted in 3C and FC trials. If animals kept its nose poke in the central port more than X s after the presentation of the visual stimuli, the trial was treated as a missing error. X was drawn from a uniform distribution with a range of [0.5, 1]. Failure to choose the correct port (left/right) within 5 s after nose withdrawal from the central port was also treated as a miss error, although it rarely occurred (< 5%). There was no punishment in any error trials, and the next trial was allowed to be initiated after ITI. In no-signal trials, animals need to wait for 0.2−0.6 s without stimulus and another 0.5−1 s to obtain a reward from the central port. There was no cue to distinguish the initial delay (0.2−0.6 s) and reward delay (0.5−1 s). Thus, animals did not have any external clue to differentiate signal trials from no-signal trials, except for the presentation of the signal itself. In FC trials, the shutter was closed 0.5 s after stimulus presentation onset, and rats were forced to choose either the left or right port (Figures 1A and 1B, bottom). In cases where no stimuli were presented in FC trials, the animals were never rewarded.

Session B followed the same protocol as session A, except that only a single stimulus difficulty was used. We applied a medium stimulus contrast level in FC trials in session A.

Electrophysiological recordings

A custom-designed electrode composed of two eight-tetrodes (tungsten wire, 12.5 μm, California Fine Wire, Grover Beach, CA) was used for the simultaneous recordings of V1 and PPC. The tetrodes were individually covered by a polyimide tube (A-M Systems, Sequim, WA), placed at a 100 μm separation, and typically had an impedance of 120–1000 kΩ at 1 kHz. The signals were recorded with Open Ephys (Cambridge, MA) at a sampling rate of 30 kHz and bandpass filtered between 0.3 and 6 kHz. The tetrodes were lowered approximately 40 μm after each recording session.

Spike sorting and screening criteria of units

All analyses were performed using MATLAB (MathWorks, Natick, MA, USA). To detect single-neuron responses, the spikes were manually clustered with MClust (A.D. Redish, University of Minnesota) for MATLAB. Only neurons that met the following criteria were included for further analyses: (1) units with sufficient isolation quality (isolation distance ≥ 15, isolation distance is a measure

Please cite this article in press as: Osako et al., Contribution of non-sensory neurons in visual cortical areas to visually guided decisions in the rat, Current Biology (2021), https://doi.org/10.1016/j.cub.2021.03.099

of unit isolation quality in high dimensional feature space from tetrode recording);[57] (2) units with reliable refractory periods (violations < 1% of all spikes); and (3) units with sufficient mean firing rates in the −0.3 – 0.5 s after cue onset (> 1 Hz).

Behavioral data analysis

Spatial choice accuracy was defined as the percentage of correct port choices in trials where either outer port was chosen upon presentation of a peripheral stimulus (Figures 1D and S1A). The miss rate was the percentage of central port choices in trials where visual stimuli were presented in 3C trials (Figures 1E and S1B). The correct rejection rate was the percentage of central choices in trials where visual stimuli were omitted in 3C trials (Figures 1F and S1C). Reaction time was defined as the duration from stimulus presentation onset to nose withdrawal from the central hole. Trials with reaction times < 100 ms were considered invalid and excluded from the calculation of spatial choice accuracy as they were considered too soon to respond to the stimulus. All error bars are presented as mean ± SEM. All violin plots combine a boxplot with a kernel density estimation procedure. The boxplot inside the violin shows the quartile, whisker, and median values as white dots (Figures S2A–S2H).

We classified the following three choice types based on the subjects' detection performance (Figures 1A–1C): (1) Hit were trials when subjects successfully chose a left or right port in 3C or before shutter closure in FC. (2) Miss-correct (Miss+) were trials when the nose remained in the central port over 0.5 s and subjects chose the correct port after shutter closure. (3) Miss-incorrect (Miss-) were trials when the nose remained in the central port over 0.5 s and subjects chose the incorrect port after shutter closure. Trials with missing responses in 3C were excluded from the analysis of comparison across choice types because they could not be categorized into Miss+ or Miss-. We set a maximum time for peripheral choice of 0.5 s∼after the shutter closed in FC trials. However, in this dataset there was no single instance where rats did not choose the peripheral port after the shutter closed.

To estimate the impact of task parameters on behavioral performance, we conducted a generalized linear model (GLM) analysis for spatial choice (left/right) and hit/miss choice (Figures 1H and S1F). In the models, we used the logit function as link function. For spatial choice GLM analysis, we prepared trials in which they performed peripheral choices. Task parameters included binary stimulus predictors (1 was stimulus presence, and 0 otherwise), previous peripheral reward (1 was rewarded, 0 otherwise), and previous central reward (1 was rewarded, 0 otherwise). The model was fit with these predictors. For hit/miss choice GLM analysis, we first prepared trials in which stimulus was present. Task parameters included binary predictors of previous peripheral reward (1 was rewarded, 0 otherwise), previous central reward (1 was rewarded, 0 otherwise), and previous failure (1 failed, 0 otherwise). Then, we fitted the model to behavioral performance using the same procedure as the spatial choice GLM analysis. To quantify the impact of each task parameter, we calculated the difference between explained variance (R^2) of the full model and partial model. The partial model lacks a target task parameter.

QUANTIFICATION AND STATISTICAL ANALYSIS

Time-locked kernel regression and visual sensitivity

To identify the task and behavioral variables of responsive neurons, we used a time-locked kernel regression approach (Figures 2A, S3A, and S3B).[58] In this approach, the firing rate of recorded neurons is described as a linear sum of task predictors aligned to task events. In this study, we considered the stimulus onset and reaction timing as task events. According to this kernel, the predicted firing rate $f_n(t)$ for a neuron n is described as

$$f_n(t) = \sum_{l}\sum_{t_s\in S} K_{l,n}(t-t_s) + \sum_{t_M\in M} K_{M,n}(t-t_M) + \sum_{t_D\in D} K_{D,n}(t-t_D) + \sum_{r}\sum_{t_R\in R} K_{r,n}(t-t_R) + \sum_{t_F\in F} K_{F,n}(t-t_F) + \sum_{w} K_{w,n}(t) + \varepsilon$$

where l represents the stimulus direction (ipsi or contra), r represents the previous reward direction (ipsi, contra, or center), w represents the whole-trial kernel types (reaction time; RT or moving time; MT) and S, M, D, R, F represents the set of times to cover each predictor window. $K_{l,n}, K_{M,n}, K_{D,n}, K_{r,n}, K_{F,n}, K_{w,n}$ represents the stimulus, motor-preparation, choice preparation, previous reward, previous failure, and whole-trial (RT or MT) kernels for neuron n. The stimulus kernels cover the window 0–0.3 s from stimulus onset, the motor preparation and choice preparation kernels cover the window −0.3–0 s from the reaction timing (central withdrawn timing), previous reward and previous failure kernels cover the window −0.1 – 0.1 s from stimulus onset. The motor preparation and the choice preparation kernels are identical except that the latter is designed to be sensitive to choice directions (ipsi-direction is a negative value). The stimulus, motor preparation, previous reward, and previous failure kernels coded as "1" or "0," and the choice preparation kernel has a value of "-1," "0," and "1," which negative and positive value indicated that ipsi- and contra-direction, zero indicated central-choice. The whole-trial kernels consist of the reaction time (RT) and moving time (MT), which has one value that remained constant for the entire trial. The values for RT and MT were min-max normalized to 0-1 range. To fit the firing rate to the model, the firing rate was binned into 0.01 s bins and then smoothed with a causal Gaussian filter with a standard deviation of 0.03 s. The stimulus (ipsi and contra) and preparation (motor and choice) kernels then contain L_S, $L_M, L_D = 30$ time bins, the previous reward (ipsi and contra) and failure kernels contain L_R, $L_F = 20$ time bins, and the whole-trial kernels (RT and MT) contain $L_W = 1$ time bins. We therefore made the design matrix DM by concatenating parameterized kernel matrices for a subset of trials of size $L \times T$ ($L = 2\times L_S + L_M + L_D + 2\times L_R + L_F + 2\times L_W = 162$ time bins, and $T = 50\times N_{trials}$ time bins) (Figure S3A).

To estimate the optimal weights for each neuron's kernels without overfitting, we estimated a weight vector w_n to solve the penalized residual sum of squares with elastic net regularization consisting of 99% L2 and 1% L1 methods during the time-locked kernel regression (using MATLAB package cvglmnet https://web.stanford.edu/∼hastie/glmnet_matlab/intro.html).[59] During weight

Please cite this article in press as: Osako et al., Contribution of non-sensory neurons in visual cortical areas to visually guided decisions in the rat, Current Biology (2021), https://doi.org/10.1016/j.cub.2021.03.099

estimation, we used the parameters in elastic net regularization λ which is calculated by minimizing cross-validated (3-fold) error within training dataset. The predicted firing rates were constructed as $P_n = DM^T w_n$.

To determine whether each neuron is sensitive to each task and behavioral kernels, we prepared a predictor matrix with full kernels (real design matrix) and a matrix in which the target kernel is set to zero within whole-time points (Partial model, Figure S3A, right). We then fit the model with each design matrix to predict firing rates and calculated the explained variance (R^2_{full}, $R^2_{partial}$) of the full and partial models, in either case with tenfold cross-validation by leaving out a random 10% subset of trials to calculate the model performance. Each fold consisted of equal proportions of contra-stimulus, ipsi-stimulus, and no stimulus emitted trials (Figure S3A, bottom). The explained variance was calculated from model-predicted and actual neuronal activity in test trials. We used an elastic-net regularization consisting of 99% L2 and 1% L1 methods during the time-locked kernel regression to prevent over-fitting.[59] If the explained variance of the partial model ($R^2_{partial}$) was significantly reduced compared to the full model (R^2_{full}), the neuron was deemed selective to the target kernel (Figure S3B, paired t test, Holm-Bonferroni correction for all comparison). Neurons selective to the stimulus contra kernel were labeled stimulus-preferring neurons, and the other neurons were labeled stimulus non-preferring neurons. Note that neurons selective to the stimulus ipsi kernel were excluded from the analyses in Figures 3, 4, 5, and 6. Nevertheless, those neurons were relatively few and their inclusion/exclusion did not affect our conclusion.

Spike train analysis

We recorded 951 neurons (V1: 515, PPC: 436 neurons) from 62 sessions in seven rats. Unless otherwise stated, the activity of each neuron was binned at 0.01 s and smoothed with a causal Gaussian filter with a standard deviation of 0.03 s to obtain the temporal profile of each neuronal activity.

For visualization (Figures 2C and S3C) and analysis, firing rates were z-scored relative to trial-by-trial baseline rates (from the window -0.5 to 0 s).

Statistics

We evaluated the statistical significance in the analysis using data resampling with a bootstrapping procedure.[60] We estimated the p value for the bootstrapping procedure by computing the ratio $(1+X) / (N+1)$, where X indicates overlapping data points between the two distributions, and N indicates iterations. Since we used 1,000 bootstraps, two distributions with no overlap resulted in $p < 0.001$, and two distributions with x% overlap resulted in $P \gg x/100$.

State-space analysis

For state-space analysis, we used neurons with $\geq$ 20 available trials for each Hit+ and Miss+ condition. To characterize the population structure and the temporal pattern among all neurons during the analysis window (-0.1 – 0.15 s from stimulus onset), z-scored firing rates were formatted as $X \in \mathbb{R}^{N \times CT}$, where N is the total number of neurons, C is the total number of conditions (choice types), and T is the number of analyzed time points. Principal component analysis (PCA) was used to reduce the dimensionality of the population from the number of neurons to ten principal components (PCs). Each PC represents a weighted combination of individual neuronal activity, which summarizes population activity.

To estimate the difference of each neural trajectory at each time point across choice types in the PC space, we prepared a dataset by bootstrapping 1,000 times with different subsets of twelve trials for each choice type. For the control dataset, trials were shuffled within Hit+ and Miss+ conditions. We then calculated the sensitivity index (d') for each PC as follows:

$$d'^2_i(t) = \frac{\left(\mu_i^{Hit+}(t) - \mu_i^{Miss+}(t)\right)^2}{\frac{1}{2}\left(\left(\sigma_i^{Hit+}(t)\right)^2 + \left(\sigma_i^{Miss+}(t)\right)^2\right)}, i \in [3(10)], t \in [-0.5\text{s}1.0\text{s}]$$

where $\mu_i^{Hit+}(t)$ and $\mu_i^{Miss+}(t)$ are the mean values of the i-th PC at time t in Hit+ and Miss+ trials, respectively, and $\sigma_i^{Hit+}(t)$ and $\sigma_i^{Miss+}(t)$ are the standard deviation of the i-th PC at time t in Hit+ and Miss+ trials, respectively. We used the sensitivity in the first three or ten PCs subspace defined as the square root of $d'^2(t)$ (Figures 3D, 3G, 3I, and S4C), as follows:

$$d'^2(t) = \sum_{3(10)} d'^2_i(t)$$

For statistical significance of the trajectories between Hit+ and Miss+ (Figures 3B, 3C, and S4B), we calculated p value as described in statistics section with the level of significance at 0.05.

State space analysis at each task and behavioral axis

For the state-space analysis at a specific task and behavioral axis (Figures 4 and S4D), we applied a variant of the "Coding Direction" analysis.[50,61] We first calculated the condition-averaged z-scored firing rate (Hit+/Miss+, or stimulus presence/absence) for each neuron for relevant epoch. To obtain the coding direction, we computed the difference of firing rates between conditions. Specifically, we defined the following four axes. The "state axis" was computed from the dissociation of neuronal activity between the Hit+ and Miss+ trials in the pre-stimulus window (-0.5 – 0 s from stimulus onset). The "movement axis" was computed from the dissociation of neuronal activity between the Hit+ and Miss+ trials in the movement window (0.3 – 0.5 s from stimulus onset). The rats moved to the contra-lateral port in the Hit+ trials because the Hit+ trials were defined as a peripheral choice before 0.5 s from stimulus onset; rather,

Please cite this article in press as: Osako et al., Contribution of non-sensory neurons in visual cortical areas to visually guided decisions in the rat, Current Biology (2021), https://doi.org/10.1016/j.cub.2021.03.099

the Miss+ trials consisted of only delayed response after 0.5 s from stimulus onset. The ''stimulus axis'' was computed from the dissociation of neuronal activity between stimulus presence and absence trials in the during-stimulus window (0 - 0.15 s from stimulus onset). Finally, the ''decision axis'' was computed from the dissociation of neuronal activity between the Hit+ and Miss+ trials in the same window (0 - 0.15 s from stimulus onset). The decision axis captures variable components such as decision formation, motor-preparation, and other subjective states. We prepared the four vectors, which are mean population activity w_a of length $N_{unit} \times 1$, indexed by the four axes. We then obtained the orthogonal axes by orthogonalizing the four vectors w_a with the QR-decomposition:

$$W = QR$$

where $W = [w_{State}\ w_{Movement}\ w_{Stimulus}\ w_{Decison}]$ is a matrix whose columns corresponding to the difference of firing rates of each axis. Q is an orthogonal matrix, and R is an upper triangular matrix. We then obtained the orthogonalized axis vectors $w_a^{\perp}$ by the first four columns of Q. These vectors span the orthogonal subspace in neuronal population activity space.

The projections of each axis were computed by dot product as $w_a^{\perp} x$, where x is an $N_{unit} \times (2 \times time)$ matrix of smoothed, trial-averaged firing rates across Hit+/Miss+ conditions.

For the statistical significance of the differences in choice-type projections for each axis, we computed the W using a subset of trials (40%) in each condition and then projected the data from the remaining subset of trials (60%) onto each axis. The procedure was repeated 100 times with shuffling trials within each condition. The sign of the projection in Hit+ was aligned to be positive in each analysis epoch. We then compared the resampling distributions between Hit+ and Miss+ or distance and zero. If the distributions are not overlapped in 2SD range (95.5% data in this range), they are defined as significantly dissociated.

To confirm whether the statistical significance of the resampling method described above is statistical noise, we conducted the simulation analysis using a noise dataset. We generated the random digits ranged -1 to 1 for 20-40 trials in two arbitrary conditions as a noise dataset and prepared 266 simulated neurons, the same number of actual data in V1. Then, the same analysis described above was performed with 100 iterations.

Classification (decoding) analysis

For classifiers, we used support vector machines (SVM) with a linear kernel function implemented using the MATLAB *fitcsvm* library. All population classification was analyzed on the concatenated neuronal activity of individual neurons. Because the number of simultaneously-recorded neurons was low in our dataset, we constructed ''pseudo-trials'' by randomly extracting trials from desired conditions for each neuron.[62] For the training and testing dataset, the number of trials in each condition was matched to prevent bias for training classifiers. We used tenfold cross-validation by leaving a 10% subset of trials for prediction to avoid overfitting. This procedure was repeated 100 times. Hyperparameter such as C regularization weight was determined by optimization to minimize loss of validation dataset in a grid search manner (searched range $10^{-5} - 10^{5}$).[63]

For two-class classification, such as stimulus classification (presence/absence) (Figure 2E) and choice type (Hit+/Miss+) (Figures 5A–5C and S5), we used the firing rate during stimulus window (0 – 0.15 s from stimulus onset) and pre-stimulus window (-0.2 – 0 s from stimulus onset) for each individual neuron, respectively. We then concatenated neuronal activity as described above and performed training and predictions. For classification metrics, we used classification improvement over shuffled (only in Hit+/Miss+ classification), which is calculated by classification accuracy in real data minus shuffled data. This ensures that high values represent the presence of neuronal information and low values represent its absence.[64] To test statistical significance, if the zero was $<$ 2SDs (95.5% distribution) of the distribution of bootstrapped classification improvement, the data was deemed significantly informative.

To classify the choice types with the simultaneously recorded population (Figures 6A and 6B), we first extracted sessions with $\geq$ 5 neurons in each region and $\geq$ 20 trials in each condition (20 sessions). We trained the classifier using the same procedure described above and predicted the test data. In the de-correlated population in V1 and PPC (Figure 6B), the trial order was shuffled within each choice type for each neuron. We then calculated the classification accuracy of real data and the de-correlated population using the procedure described above.

To measure the contributions of each neuron for the choice types (Figure 5D), we compared weight distributions of the classifier for different neuronal types, that is, contra-stimulus selective neurons and the other selective neurons. The neuronal weight was normalized to unity length. For statistical significance, we performed a one-way ANOVA test with LSD post hoc comparisons.

Stability (cross-temporal classification analysis)

To estimate the stability of population coding, we applied a cross-temporal classification analysis where the classifiers were trained and tested with unique time samples (Figure S5). Each classifier trained at time $t_{trained}$ can also be tested on its classification ability to predict the choice outcome at time t_{tested}. For visualization, we computed the classification improvement over shuffled data as described above (see classification analysis). The negative value was rounded to zero, and the above 0.5 value was rounded to 0.5. When we test the statistical significance of predictability, we used the same metrics with the classification improvement described above using unrounded value.

To estimate the stability of population coding, we calculated Pearson's correlation coefficients between the neuronal weights of each classifier at time $t_{trained}$ and t_{tested} (Figures S5C and S5D). To quantify the time-resolved decay of population activity pattern, we used Pearson's correlation coefficients 0 – 0.5 s from time $t_{trained}$ (Figure S5D) in -0.2 s–0 s training time. For comparison between populations, we used Kolmogorov–Smirnov test followed by post hoc Tukey tests for subpopulations and regions (Figure S5D).

Please cite this article in press as: Osako et al., Contribution of non-sensory neurons in visual cortical areas to visually guided decisions in the rat, Current Biology (2021), https://doi.org/10.1016/j.cub.2021.03.099

Noise correlation

Noise is defined as the trial-to-trial variability of the neural response from the mean under a given choice type condition. Noise correlation was defined as the correlation coefficient between the noise of a given neuron pair within the same choice type conditions. Specifically, we arranged the firing rates of single neurons in a trial-by-time matrix per choice type with a time resolution of 50ms spanning −0.4 – +0.4 s after the stimulus onset. The matrix was z-scored with the mean and the standard deviation of the trials at each time point for each choice type. Then, we calculated Pearson's correlation coefficients of the z-scored firing rates (i.e., noise) for each pair of neurons at each time point (Figures 6C, 6D, and S6C).

Cell-type classification

To classify the putative fast-spiking (FS) interneuron and regular-spiking (RS) excitatory neurons, we calculated trough to late peak and firing rate for each recorded unit (Figures S6A and S6B). We then determined the cell types by clustering the units in the dimension of the parameters using the k-means algorithm (k = 2) with these two variables using the MATLAB *kmeans* function. After clustering units, we defined clusters that had a lower trough to late peak compared to the other cluster as putative FS interneurons and the other as RS excitatory neurons.